RSC Advances

ROYAL SOCIETY OF CHEMISTRY

www.rsc.org/advances

Journal Name

ARTICLE

Co_3O_4 Nanoparticles grown on N-doped Vulcan Carbon as Scalable Bifunctional Electrocatalyst for Rechargeable Zinc-Air Batteries

Received 00th January 20xx,
Accepted 00th January 20xx

DOI: 10.1039/x0xx00000x

www.rsc.org/

Tao An,[a] Xiaoming Ge,[a] T. S. Andy Hor,[a,b,*] F. W. Thomas Goh,[a] Dongsheng Geng,[a] Guojun Du,[a,b] Yi Zhan,[c] Zhaolin Liu,[a,*] and Yun Zong[a,*]

Bifunctional electrocatalysts for rechargeable metal-air batteries often encounter catalyst leaching-resultant performance degradation upon cycling of batteries, which requires stability improvement on catalyst nanoparticles via immobilization onto conductive supports. Herein, we report in-situ growth of Co_3O_4 nanoparticles onto the concurrently synthesized N-doped Vulcan carbon (NVC) to produce Co_3O_4/NVC powders with tuneable loading density as scalable, stable and efficient hybrid bifunctional electrocatalysts. With optimized composition the hybrid catalyst exhibited satisfactory ORR and OER activity, giving a voltage difference as small as 0.10 V between the onset potential and half-wave potential at discharge. The good performance of the rechargeable zinc-air batteries constructed using Co_3O_4/NVC as air-cathodes suggests such hybrid bifunctional electrocatalyst as a practical and cost-effective solution for applications with large quantity materials demand, e.g. in grid-scale energy storage and electric vehicles.

Introduction

Air-pollution has become a dreadful issue in many developing countries, to which the exhaust gas out of automobiles with gasoline or diesel-based combustion engines have contributed significantly. Electric vehicles (EVs), powered by electricity of rechargeable battery packs, are proposed as a good solution to mitigate such issues.[1] This shift of vehicle power source away from gasoline and diesel, however, further imposes pressure on the ever-increasing demand of electricity supply by modern societies with high civilization. Electricity harvested from some non-traditional energy sources, e.g. solar, wind, and thermal energies can be utilized to cover the deficiency, requiring good match of electricity supply with demand in the timeframe via smart grid storage, to which safe, durable and cost-effective battery technology is the key.[2]

The most advanced battery technology in the market, i.e. lithium-ion (Li-ion) battery, typically offers an energy density of 120-200 Wh kg^{-1}.[3,4] The high energy efficiency makes them an ideal choice for devices with a need of small scale energy storage, e.g. consumer electronics. For grid storage application that requires giant battery pack systems, the large volume of flammable electrolytes used therein will become serious safety concerns.[5] Recent progress in aqueous based secondary Li-ion batteries is encouraging;[6-8] however, the commercial viability, cost-effectiveness, and durability are still in question. A higher energy density and safer alternative, e.g. zinc-air battery using metallic zinc anode, oxygen cathode and aqueous electrolyte, is promising in perspective, yet commercial success was only seen in primary cells so far. Their rechargeable counterparts are facing practical challenges, e.g. poor rechargeability and low energy efficiency. These issues may be mitigated by raising the coulombic efficiency and lowering the overpotential of Zn-air batteries, which may be partially achievable by employing an efficient bifunctional catalyst on air-cathode that facilitates the oxygen reduction reaction (ORR) and oxygen evolution reaction (OER) in the discharge and charge of the batteries, respectively.[9-11]

Nobel metals with their high cost and scarcity are by no means suitable to be used as bifunctional catalysts for zinc-air batteries. Exploitation on their cost-effective alternatives has led to the discovery of a number of metal oxides with either spinel [12-16] or perovskite [17-21] structures that efficiently catalyse OER. Co_3O_4, a representative simple and single metal oxide of spinel structure is especially prominent for its low cost and high abundance yet promising OER catalytic activity in alkaline solutions.[12,14] Nanostructured Co_3O_4 can be readily synthesized via methods of sol-gel,[22] combustion,[23] spray pyrolysis [24] and hydrothermal reactions.[25,26] The low ORR activity of Co_3O_4 can

[a] Institute of Materials Research and Engineering (IMRE), A*STAR (Agency for Science, Technology and Research), 3 Research Link, Singapore 117602, Republic of Singapore. E-mails: zl-liu@imre.a-star.edu.sg, y-zong@imre.a-star.edu.sg

[b] Department of Chemistry, National University of Singapore, 3 Science Drive 3, Singapore 117543, Republic of Singapore. E-mail: andyhor@nus.edu.sg

[c] Department of Chemical and Biomolecular Engineering, National University of Singapore, 4 Engineering Drive 4, Singapore 117576, Republic of Singapore

be addressed by bringing it into contact with Ag,[27] Ni[28] or MnO_2,[29] etc. More recently, people started to integrate spinel Co_3O_4 nanoparticles with carbonaceous materials of good electrical conductivity whose ORR activity is further boosted via doping with heteroatom of N, O, B, S, P, etc.[30-35] In particular, it was reported that N-doping into graphene led to superior ORR catalysts as the N atoms introduced into the graphene lattice promoted the neighbouring carbon atoms to "active regions" with enhanced electrocatalytic activity.[36] The types of carbon materials studied include carbon nanoweb,[30] mesoporous carbon,[31] carbon nanofibers[32] and nanotubes,[33-35] etc., whereby superior ORR and OER activities were observed unanimously.

Despite of all these successes, the special structured carbons could have cost implication for applications with huge quantity of catalyst demand, e.g. in grid-storage or electrical vehicles. Herein, we report Co_3O_4 nanoparticles loaded N-doped Vulcan carbon (Co_3O_4/NVC), prepared by in-situ growth of Co_3O_4 NPs onto the concurrently synthesized NVC under hydrothermal conditions, as efficient oxygen catalyst. The loading density of Co_3O_4 was tuned by controlling the concentration of Co(III) precursors in the starting materials. The resultant composite catalysts were characterized, with their ORR and OER catalytic activities being evaluated and compared with benchmark Pt/C and manually mixed Co_3O_4 and VC or NVC. The performance of Co_3O_4/NVC in zinc-air batteries was also evaluated.

Experimental

Preparation of composite catalysts. The Co_3O_4/NVC composites were synthesized via in-situ growth of Co_3O_4 onto concurrently synthesized NVC from Vulcan XC-72 carbon black powder (VC, Cabot Corporation, USA) under hydrothermal conditions. In a typical reaction, 16.0 mg VC was homogeneously dispersed into 50 ml ethanol under sonication, prior to the addition of calculated amount of cobalt (III) acetyl acetonate (99.99%, Aldrich, USA). Upon the introduction of 1 ml aqueous $NH_3 \bullet H_2O$ (35.0 wt%), the reaction mixture was transferred into a Teflon vessel and sealed in stainless steel autoclave to allow for 3 h of reaction at 150°C. The product was collected by centrifugation, washed with ethanol and deionized water, and dried over a freeze-dry process. NVC was synthesized following the same procedure except the addition of Co(III) precursor. As control, commercial Co_3O_4 nanopowders (<50 nm, 99.5%, Aldrich, USA) were manually mixed with VC or NVC in a weight ratio of 2:3 using agate mortar and pestle, and benchmark catalyst Pt/C (20 wt% Pt on VC) was purchased from Alfa Aesar (USA).

Material characterizations. The loading density of Co_3O_4 in the hydrothermally synthesized Co_3O_4/NVC was determined on a thermogravimetric analyzer (TGA, Q500, TA Instruments) at a temperature ramp rate of 25°C min^{-1}. X-ray diffraction (XRD) study was performed on a Bruker D8 Advance diffractometer with Cu K_α radiation (λ = 1.5406 Å) to determine the crystal structure and phase of Co_3O_4. Raman spectra of Co_3O_4/NVC were recorded from a Renishaw inVia Raman microscope, and their morphology feature was studied using a field emission scanning electron microscope (FESEM, JEOL-7600F) and a transmission electron microscope (TEM, Philips CM300). X-ray photoelectron spectroscopy (XPS) data were collected on a VG ESCALAB 200i-XL XPS system with Al K_α radiation (hν = 1486.6 eV), and correction to binding energies was made according to the C 1s line at 285.0 eV from adventitious carbon.

Electrochemical measurements. The catalytic activities of the obtained Co_3O_4/NVC toward ORR and OER were assessed with a three-electrode half-cell setup comprising a rotating disc electrode (RDE) as the working electrode, Pt foil as counter electrode and Ag/AgCl in 3.0 M KCl solution as reference electrode. To prepare the working electrode, ink was formed by mixing 5 mg of each respective catalyst and 25 µl Nafion perfluorinated resin solution (5 wt%, Aldrich, USA) in 923 µl ethanol, followed by sonication for 1 h. 10 µl of the respective ink was dropped onto a glassy carbon electrode (5 mm in diameter) and dried naturally to achieve a loading of 0.25 mg cm^{-2}. The electrodes were then immersed into 0.1 M KOH aqueous solution and purged with ultrapure oxygen gas prior to the experiment. An Autolab PGSTAT302N was used for data collection, and a constant flow of oxygen gas was maintained during the experiment. The working electrode was scanned at 5 mV s^{-1} with a series of rotation rates (400-2500 rpm) being employed. NVC, mechanical mixtures of Co_3O_4 with VC or NVC, i.e. Co_3O_4+VC and C_3O_4+NVC, as well as the benchmark Pt/C catalyst were studied under same condition for comparison purpose.

To further evaluate the catalytic performance and durability of Co_3O_4/NVC catalysts, battery cycling tests were performed using home-made zinc-air cell device that has been described in details previously.[37] In brief, the cathode was prepared by spreading the catalyst slurry onto carbon paper (SGL 10BC, Germany) to achieve a loading density of 4.0 mg cm^{-2}, with the working area of the air cathode being 4 cm^2. Metallic zinc plate was employed as the anode, with 6.0 M KOH aqueous solution containing 20.0 g L^{-1} $ZnCl_2$ as the electrolyte. The battery tests were carried out at 25 °C on a Maccor 4300 battery tester. In each test cycle, the cell was discharged at a constant current of 20 mA over 4h and then charged at a constant current of 10 mA over 8 h.

Results and discussion

In the synthesis of Co_3O_4/NVC, Co_3O_4 may grow on NVC to form the target product, or appear as free nanoparticles in the suspension. As Co_3O_4/NVC was collected via centrifugation at the end of the reaction, majority of the free small Co_3O_4 NPs remained in the supernatant. Washing process removed the rest of the free particles and left mostly only those firmly attached Co_3O_4 in the final composite products. Since not all Co_3O_4 produced were attached onto NVC, its content in the

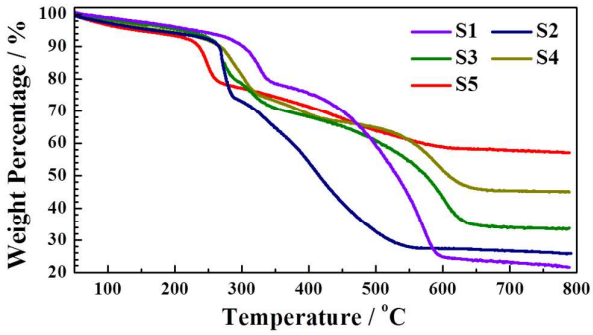

Figure 1 TGA data of the Co_3O_4/NVC hybrids with various amounts of cobalt (III) acetyl acetonate used as starting materials in the synthesis. The initial loss of 10 wt% is attributed to the removal of incorporated moisture water.

resultant hybrids would unlikely satisfy a linear relationship to the initial inputs of the cobalt (III) acetyl acetonate. The actual Co_3O_4 content in the obtained hybrids was thus quantified via thermogravimetric analysis (TGA), and the data curves are presented in Figure 1. The initial weight loss up to 300 °C likely accounted for the absorbed water and amorphous carbons in the samples. The calculated Co_3O_4 content of all 5 samples (using dehydrated mass as the base weight) are presented together in Table 1.

One can see that the Co_3O_4 content was elevated with the increased concentration of $Co(acac)_3$ in the starting materials, and a content of over 60 wt% was easily achievable. At lower $Co(acac)_3$ concentration (1.76 mM), majority of the as-formed Co_3O_4 NPs (73.1%) tended to adhere onto NVC, showing good compatibility of the two materials. As the concentration of $Co(acac)_3$ was elevated, the percentage of Co_3O_4 formed as free nanoparticles gradually increased as a collective effect of increasing stereo barrier to the further growth of Co_3O_4 onto NVC and the higher reactivity from the increased reactant concentration in the solution. At further increased $Co(acac)_3$ concentration (22.4 mM) the on-NVC-grown Co_3O_4 eventually was turned into the minority (30.7%). Nevertheless, the overall Co_3O_4 content on NVC was steadily elevated with the increase of $Co(acac)_3$ concentration, and a loading density of 63.3 wt% was achieved which was sufficiently high to study on the effect of catalyst content in rechargeable zinc-air batteries.

Table 1 Initial concentration of $Co(acac)_3$ in the synthesis of Co_3O_4/NVC and the corresponding residual content from TGA data in Figure 1. The Co_3O_4 content in Co_3O_4/NVC and the yield of Co_3O_4 on NVC were calculated by dividing the respective residue mass with its dry Co_3O_4/NVC mass or 100% yield mass of Co_3O_4 based on the inputs of Co(III) precursor, respectively.

Sample No.	Initial $Co(acac)_3$ Conc. (mM)	Residual Content (wt %)	Co_3O_4 Content in Co_3O_4/NVC (wt %)	Yield of Co_3O_4 on NVC (%)
1	1.76	22	24.4	73.1
2	2.74	26	28.9	59.1
3	4.12	34	37.8	58.8
4	9.60	45	50.0	41.5
5	22.4	57	63.3	30.7

From the SEM image in Figure 2a one can see that NVC particles generally were in the size of tens of nanometers in the absence of Co_3O_4 NPs. With the introduction of Co_3O_4 via the Co(III) precursor, composite particles of Co_3O_4/NVC were formed in a notably bigger size (Figure 2b). Further increase of Co_3O_4 content led to the formation of large Co_3O_4 flakes covering NVC (Figure 2c). The zoom-in view of a single particle of Co_3O_4/NVC under a high resolution transmission electron microscope (HR-TEM) gave spherical Co_3O_4 NPs of 2-3 nm in diameter on the surface with lattices of different orientations (Figure 2d). These small but highly crystalline Co_3O_4 anchored on conductive N-doped Vulcan carbons would be ideal for catalytic application due to their large surface area and good electrical conductivity.

The X-ray diffraction patterns of the blank NVC and a representative Co_3O_4/NVC are shown in Figure 3a. For NVC two major diffraction peaks at 24.7° and 43.2° are clearly visible (bottom curve), which can be assigned to the (002) and (101) planes of hexagonal graphite.[38] This suggests that the crystallographic structure of VC was retained after the N-doping. In the case of Co_3O_4/NVC, the Cu target in the X-ray tube induced strong fluorescence on cobalt sample[39] and thus high background noise which compromised the resolution of the obtained diffraction patterns of the sample. Nonetheless, the major diffraction peaks identifiable pointed to the spinel structure of Co_3O_4 (top curve). The unpronounced diffraction peaks of NVC in Co_3O_4/NVC were likely due to the suppressed diffraction intensity by the high loading of Co_3O_4 grown on the

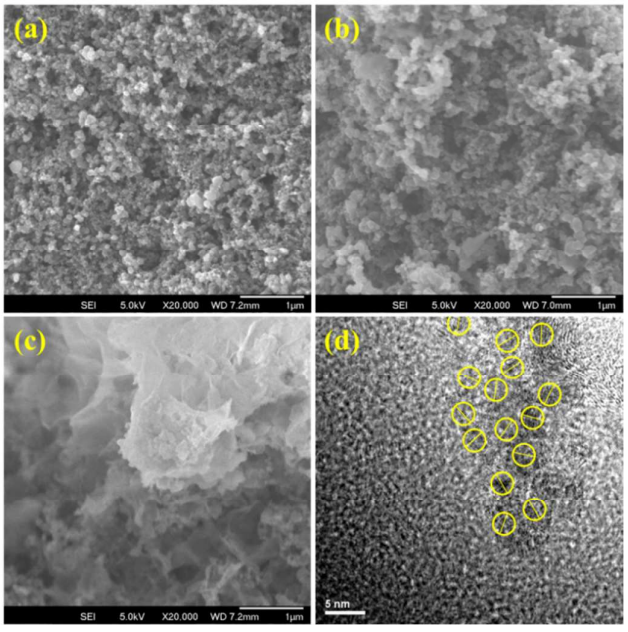

Figure 2 SEM images of (a) blank N-doped Vulcan carbon (NVC), (b) Sample 2 (with second lowest Co_3O_4 loading), (c) Sample 5 (with highest Co_3O_4 loading) and (d) a representative HR-TEM image of the Co_3O_4/NVC hybrids. Nanoparticles with different orientations of lattices can be seen inside the small yellow circles.

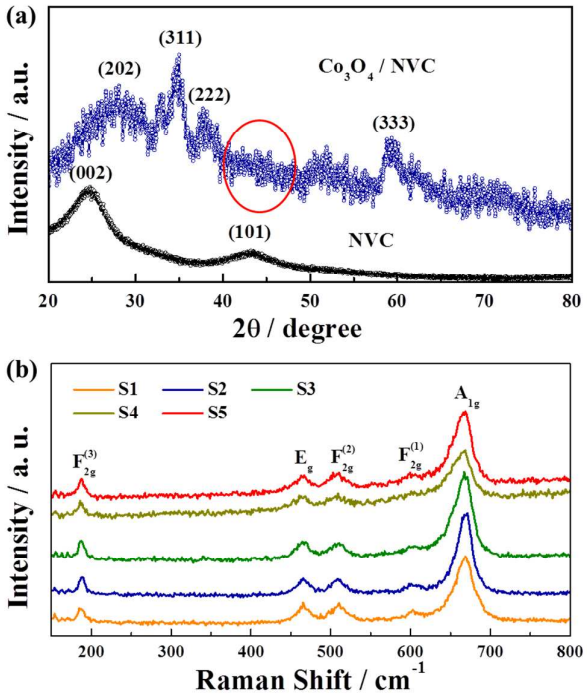

Figure 3 (a) Representative *X*-ray diffraction (XRD) patterns of Co_3O_4/NVC with the major diffraction peaks suggesting spinel Co_3O_4 (top curve) and that of NVC (bottom curve). (b) Ramam spectra of all 5 Co_3O_4/NVC samples with varied loading of Co_3O_4.

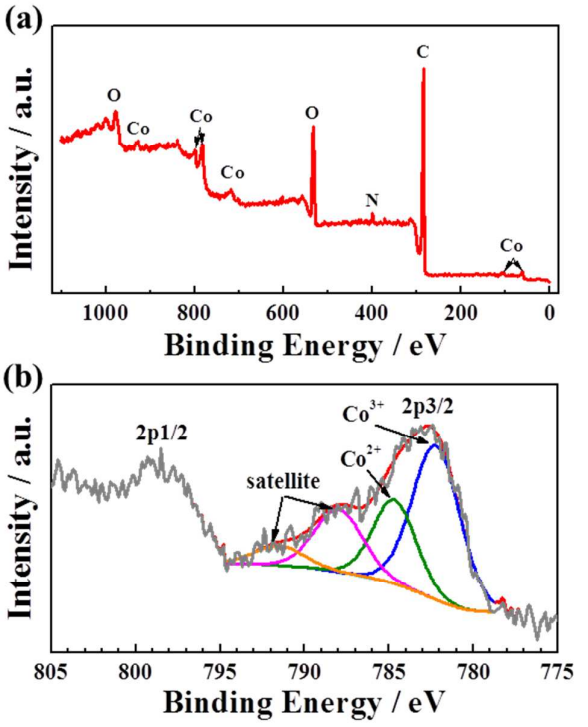

Figure 4 XPS spectra of (a) full range survey and (b) Co 2p high resolution scan of Co_3O_4/NVC. The satellites peaks were probably due to the interactive bonding between Co_3O_4 and Vulcan carbon.

top of NVC. These signals appeared even weaker under the strong fluorescence background noises induced by Cu K_α radiation on Co-based samples. Nevertheless, if one compares the diffraction patterns of NVC and Co_3O_4/NVC in Fig. 3a, it is not difficult to conclude that in Co_3O_4/NVC the diffraction peak (002) of NVC at 24.7° in fact joined the (202) peak of spinel Co_3O_4 to form a broader peak, while the diffraction peak (101) at 43.2° was identifiable (inside the red oval) despite of a relatively low intensity. To further confirm the formation of Co_3O_4, Raman spectra were collected in the range of 150 - 800 cm^{-1} and five bands with symmetry modes A_{1g}, E_{2g} and 3 F_{2g}, respectively, can be identified (Figure 3b). These bands were almost identical for all five samples and matched very well with that of spinel Co_3O_4,[40,41] confirming successful synthesis of Co_3O_4/NVC as suggested by the XRD data.

The XPS survey scan data (Figure 4a) indicates the presence of Co, O, C and N in the as-prepared samples, and the N 1s peak at the binding energy of 400 eV is likely from graphitic N. The N content in NVC was determined to be 3.2 at%, which is comparable to that of NH_3-treated mesoporous carbon.[31] Such moderately high content of graphitic N in the Co_3O_4/NVC samples is favourable to high ORR catalytic activity. Figure 4b shows the high resolution spectrum of Co 2p, where Co $2p_{3/2}$, Co $2p_{1/2}$ and the associated satellite peaks can be readily identified. The deconvolution of Co $2p_{3/2}$ revealed the ratio of integrated area between Co^{2+} and Co^{3+} peaks as 1:2.03, which is in good agreement with their theoretical atomic ratio of 1:2 as in Co_3O_4.

The ORR and OER activities of the five C_3O_4/NVC samples were evaluated using RDE technique, with Pt/C, NVC, Co_3O_4+VC and C_3O_4+NVC being measured for comparison. At a rotation speed of 1600 rpm, the C_3O_4/NVC samples attained their onset potentials as -0.08, -0.08, -0.09, -0.11 and -0.13 V, respectively (Figure 5a), whereby the slight increase of the on-site potential from Sample 1 to 5 is likely associated with the gradually decreased content of NVC in these samples. It is envisaged that higher NVC content helps improve the electrical conductivity of Co_3O_4/NVC, enabling more efficient electron transfer and spillover phenomena in ORR. For NVC content of as high as 75.6 wt % (Sample 1) and 71.1 wt% (Sample 2), similar onset potential of -0.08 V with limiting current density of 4.6 ± 0.1 mA cm^{-2} at -0.8 V were achieved, which are rather close to that of the benchmark Pt/C with onset potential of -0.02 V and limiting current density of 5.2 mA cm^{-2} at -0.8 V.

On the other hand, blank NVC displayed an inferior onset potential of -0.15 V to those of the Co_3O_4/NVC hybrids. Although Co_3O_4 is generally considered as an OER catalyst, the synergetic effect between Co_3O_4 and NVC was found to drive the ORR activities of the Co_3O_4/NVC hybrids beyond that of blank NVC. Also, compared to Co_3O_4/NVC, the mechanical mixture of Co_3O_4 with VC or NVC (w/w: 2:3), i.e., Co_3O_4+VC and C_3O_4+NVC, showed inferior onset potential of -0.18 V and -0.17 V, respectively, due to the lack of synergetic effects between Co_3O_4 and NVC therein which largely failed the requirement of close contact of the two components. The half-wave potential, E½, of the Samples 1-5 was measured to be -0.18, -0.18, -0.18,

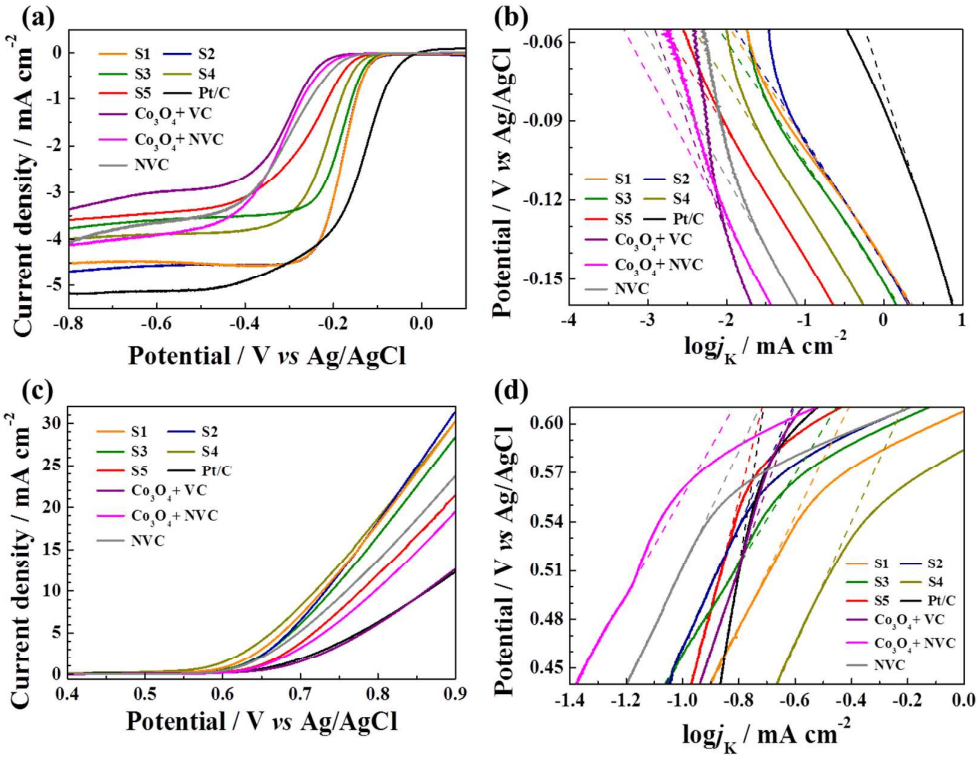

Figure 5 The (a) ORR and (c) OER voltammetric curves of the Co_3O_4/NVC as compared to Pt/C, NVC, and mixture of commercial Co_3O_4 with VC or NVC, and the corresponding Tafel plots of (b) ORR and (d) OER curves. The Tafel plots are fitted in linear-least-squares at lower potentials.

-0.21 and -0.25 V, respectively. These values appear inferior to that of Pt/C (-0.14 V), while the smaller difference between onset potential and E½ for Samples 1-4 as compared to that of Pt/C (0.10 *vs* 0.12 V) indicates their good catalytic activities. Moreover, Tafel slopes of Samples 1-5 are found as 45, 47, 46, 48 and 49 mV/dec, respectively, which are notably smaller than that of Pt/C (93 mV/dec) and the blank NVC (54 mV/dec) (Figure 5b), suggesting higher current density achievable at lower overpotential which is in favour of electrocatalytic ORR applications.

For OER, the Co_3O_4/NVC gives a similar onset potential of 0.55 V (Figure 5c) for Co_3O_4 content of 24.4 to 37.8 wt%. At 50 wt% Co_3O_4 the onset potential drops to 0.50 V which seems to suggest that high Co_3O_4 content helps lower onset potential. However, Sample 5 with 63.3 wt% of Co_3O_4 gives an onset potential of 0.60 V, which is at the similar level to that of Pt/C and mechanical mixture of commercial Co_3O_4 and VC or NVC. The cause of this abnormality is likely the significantly decreased electrical conductivity at such high Co_3O_4 content. Another interesting finding is that Samples 1-4 show similar current density of 30 ± 1.5 mA cm^{-2} at 0.9 V, which is notably higher than those of Pt/C, NVC, and commercial Co_3O_4+VC and Co_3O_4+NVC mixtures. As anticipated Sample 5 with a higher onset potential shows a lower current density as compared to its counterparts with lower Co_3O_4 content. Similarly, Samples 1-4 give similar Tafel slopes of 0.28-0.38 V/dec, which are much smaller than that of Sample 5 (0.68 V/dec) or Pt/C (1.12 V/dec). Surprisingly, blank NVC (0.36 V/dec) and the mixture of commercial Co_3O_4 with VC (0.50 V/dec) or NVC (0.30 V/dec) display smaller Tafel slopes as compared to Sample 5 (0.68 V/dec), suggesting notable advantage of a higher content of NVC (possibly also a higher electric conductivity). Therefore, taking into account of the onset potential, cathodic current density and Tafel slope, we can conclude that the optimal ORR and OER activities could be established at a composition of 30 wt% Co_3O_4 and 70 wt% NVC, which is close to the case in Sample 2.

It should be noted that the current density recorded in RDE is a function of rotation rate, as higher rotation rate leads to faster oxygen diffusion and thus a higher current. This relationship was defined by the Koutecky-Levich equation of[42]

$$j^{-1} = j_k^{-1} + j_l^{-1} \quad (1)$$

where j_k is the kinetic current density and j_l is the Levich current density, and the latter is defined as[43]

$$j_l = 0.201nFCD^{2/3}\nu^{-1/6}\varpi^{1/2} \quad (2)$$

where n is the electron transfer number, F is Faraday constant,

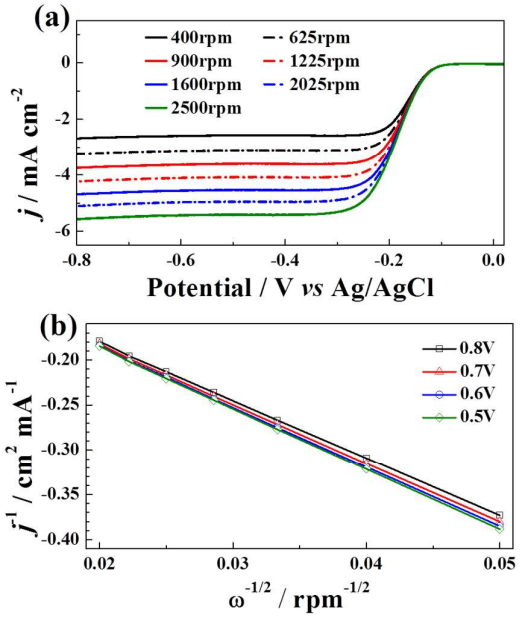

Figure 6 (a) Rotating-disk voltammogram of Sample 2 at various rotation speeds and (b) the Koutecky-Levich plots at 0.5-0.8 V. It had a high half-wave potential of -0.18 V, which was only 0.1 V from the onset potential (-0.08 V).

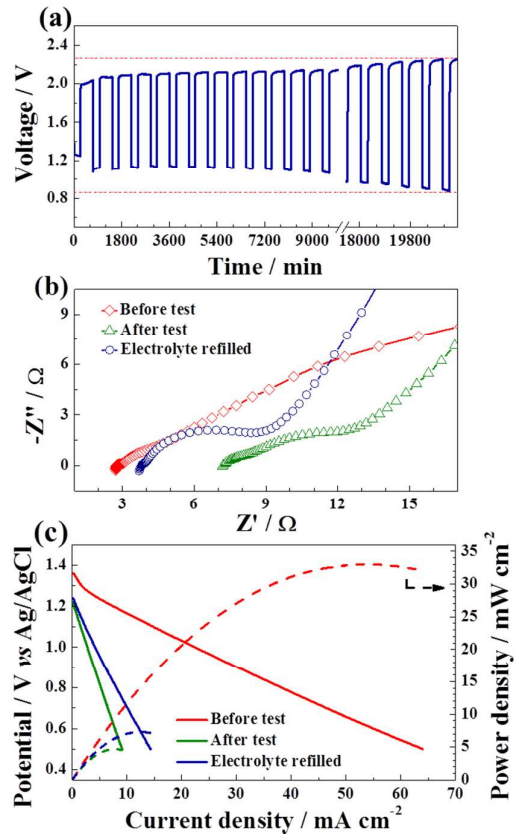

Figure 7 (a) The battery test data at constant-current charge-discharge cycling; (b) the battery impedance; (c) V-I curves (solid lines) and the output power density (dash lines) at discharge measured before the battery test, right after the test and with the electrolyte refilled.

C is the concentration of dissolved oxygen in the electrolyte, D is oxygen diffusion coefficient, ν is electrolyte kinetic viscosity, and ϖ is the electrode rotation rate in rpm. For 0.1 M KOH aqueous solution saturated with O_2 at 25 °C, D = 1.9 × 10^{-5} cm^2 s^{-1},[44] ν = 0.010 cm^2 s^{-1},[45] and C = 1.2 × 10^{-6} mol cm^{-3}.[44] The electron transfer number can be calculated from the slope of the linear plot of j^{-1} against $\varpi^{-1/2}$. For Sample 2, the current density at various potential was extracted from the rotating-disk voltammograms (Figure 6a) to produce Koutecky-Levich plots (Figure 6b). The number (n) of electrons transferred per oxygen molecule was calculated from these plots to be 4, in agreement with that of Co_3O_4/N-doped graphene hybrids.[14] This favourable 4-electron transfer reaction pathway for ORR is superior to the two-electron transfer reaction pathway for the sake of not only the higher efficiency, but also the mitigated detrimental peroxide species.[10]

To further evaluate the performance of hybrid Co_3O_4/NVC catalysts, Sample 2 was taken and employed on air cathode of a rechargeable zinc-air cell which was tested on discharge-charge cycling over 15 days (Figure 7a). It was found that the discharge voltage remained above 1.1 V with charge voltage below 2.1 V in the first 4 days. However, at the end of 15 days a big portion of the electrolyte leaked out with the discharge and charge voltages reached 0.85 and 2.25 V, respectively. The high-frequency impedance was found to be 7.2 Ω (Figure 7b), which is notably higher than that of the freshly assembled cell prior to test (2.7 Ω). As soon as the cell was refilled with fresh electrolyte of KOH/$ZnCl_2$, a high- frequency impedance of 3.8 Ω was obtained which is higher than that of freshly assembled cell yet substantially lower as compared to cell with electrolyte half-filled. Prior to the cycling test, a current density of 64 mA cm^{-2} was achieved as the cell was discharged to 0.5 V, whereby a maximum power density (P_{max}) of 33 mW cm^{-2} was seen at the discharge current density of 53 mA cm^{-2} (Figure 7c). On the 15th day as the cell malfunctioned, the discharge current density dropped to 9 mA cm^{-2} at the potential of 0.5 V which, however, increased to 14.3 mA cm^{-2} with the refill of fresh electrolyte. As this value is significantly lower than that of the freshly assembled cell, we can conclude that the deterioration of the cell was only partially due to the loss of electrolyte during the charge-discharge cycling. Leaching of the catalysts off the air cathode and the corrosion of carbon blacks at high charging voltages should have caused more damages here, as evidenced by a clear electrolyte colour change from colourless to blackish. These issues are to be solved in future work, so that high-performance rechargeable zinc-air batteries with no electrolyte leakage but strong adhesion of catalysts to carbon paper and corrosion-resistant layers, with highly hydrophobic and hydrophilic nature at either side, and ample gas diffusion channels are achievable.

Conclusions

In summary, a series of Co_3O_4 nanoparticles decorated NVC composite catalysts have been successfully synthesized via a robust hydrothermal method, with the Co_3O_4 to NVC ratio

being tuned by vaying concentration of Co(III) precusor which was eventually determined by TGA. The formation of Co_3O_4 was evidenced by the characteristic peaks in Raman spectra with their spinel structure revealed by XRD. XPS confirmed successful doping of N into VC, and the content of graphatic N was about 3.2% which is moderately high for a good ORR catalytic activity. SEM and HRTEM images suggested NVC particles as spheres of a few tens of nanometers, with the size of the incorporated Co_3O_4 nanoparticles being 2-3 nm. RDE test results suggested the optimal Co_3O_4/NVC composition as 30 wt% Co_3O_4 and 70 wt% NVC that led to the best overall performance. Its ORR onset potential was close to that of the benchmark Pt/C catalyst, with the difference between onset potential and half-wave potential being smaller which suggests good ORR activity. It was also far superior to blank NVC, and the manually mixed Co_3O_4 nanopowders with VC or NVC, showing the importance of a synergetic effect arising from vicinity of Co_3O_4 to NVC achieved via direct growth approach. Unsurpringly, for OER catalytic activity Co_3O_4/NVC notably outformed Pt/C. The use of commercial Vulcan carbon black as the base material allowed for large scale synthesis of such composite catalysts without any notable compromise on their electrocatalytic activities towards ORR and OER. This was evidenced by the reasonably good discharge-charge cycling behavior observed on a home-made zinc-air battery employing Co_3O_4/NVC with optimized composition as the air-cathode catalyst. Co_3O_4/NVC hybrid represents an efficient, durable, cheap and scalable bifunctional electrocatalyst, shedding a light on commercial development of rechargeable zinc-air batteries.

Acknowledgements

This work was supported by the projects IMRE/12-2P0503 and IMRE/12-2P0504 under the SERC Advanced Energy Storage Research Programme, and Institute of Material Research and Engineering (IMRE), A*STAR, Singapore. We thank Ms. Ong Lay Ting June (IMRE) for XPS data collection, Ms. Tan Hui Ru (IMRE) for assistance in TEM characterization and Dr Martin K. Schreyer (ICES) for XRD measurements and advice.

Notes and references

1 U. Eberle, R. von Helmolta, *Energy Environ. Sci.*, 2010, **3**, 689.
2 D. Lindley, *Nature*, 2010, **463**, 18.
3 J. M. Tarascon, M. Armand, *Nature*, 2001, **414**, 359.
4 J. B. Goodenough, Y. Kim, *Chem. Mater.*, 2010, **22**, 587.
5 M. A. Rahman, X. Wang, C. Wen, *J. Electrochem. Soc.*, 2013, **160,** A1759.
6 J. Y. Luo, W. J. Cui, P. He, Y. Y. Xia, *Nat. Chem.*, 2010, **2**, 760.
7 H. Kim, J. Hong, K.-Y. Park, H. Kim, S.-W. Kim, K. Kang, *Chem. Rev.*, 2014, **114**, 11788.
8 N. Alias, A. Z. Mohamad, *J. Power Sources*, 2015, **274**, 237.
9 V. Neburchilov, H. Wang, J. J. Martin, W. Qu, *J. Power Sources*, 2010, **195**, 1271.
10 F. Cheng, J. Chen, *Chem. Soc. Rev.*, 2012, **41**, 2172.
11 Y. Li, H. Dai, *Chem. Soc. Rev.*, 2014, **43**, 5257.
12 M. Hamdani, R. N. Singh, P. Chartier, *Int. J. Electrochem. Sci.*, 2010, **5**, 630.
13 F. Cheng, J. Shen, B. Peng, Y. Pan, Z. Tao and J. Chen, *Nat. Chem.*, 2011, **3**, 79.
14 Y. Liang, Y. Li, H. Wang, J. Zhou, J. Wang, T. Regier, H. Dai, *Nat. Mater.*, 2011, **10**, 780.
15 M. Prabu, K. Ketpang, S. Shanmugam, *Nanoscale*, 2014, **6**, 3173.
16 X. Ge, Y. Liu, F. W. T. Goh, T. S. A. Hor, Y. Zong, P. Xiao, Z. Zhang, S. H. Lim, B. Li, X. Wang, Z. Liu, *ACS Appl. Mater. Interfaces*, 2014, **6**, 12684.
17 A. Weidenkaff, S. G. Ebbinghaus, T. Lippert, *Chem. Mater.*, 2002, **14**, 1797.
18 N. L. Wu, W. R. Liu, S. J. Su, *Electrochim. Acta*, 2003, **48**, 1567.
19 K. N. Jung, J. H. Jung, W. B. Im, S. Yoon, K. H. Shin, J. W. Lee, *ACS Appl. Mater. Interfaces*, 2013, **5**, 9902.
20 D. U. Lee, H. W. Park, M. G. Park, V. Ismayilov, Z. W. Chen, *ACS Appl. Mater. Interfaces*, 2015, **7**, 902.
21 X. Ge, F. W. T. Goh, B. Li, T. S. A. Hor, J. Zhang, P. Xiao, X. Wang, Y. Zong, Z. Liu, *Nanoscale,* 2015, **7**, 9046.
22 M. El Baydi, G. Poillerat, J.-L. Rehspringer, J. L. Gautier, J.-F. Koenig, P. Chartier, *J. Solid State Chem.*, 1994, **109**, 281.
23 F. Gu, C. Li, Y. Hu, L. Zhang, *J. Cryst. Growth*, 2007, **304**, 369.
24 D. Y. Kim, S. H. Ju, H. Y. Koo, S. K. Hong, Y. C. Kang, *J. Alloys Compd.*, 2006, **417**, 254.
25 D. U. Lee, J. Scott, H. W. Park, S. Abureden, J.-Y. Choi, Z. W. Chen, *Electrochem. Commun.*, 2014, **43**, 109.
26 S. Huang, Y. Jin, M. Jia, *Electrochim. Acta*, 2013, **95**, 139.
27 H. M. A. Amin, H. Baltruschat, D. Wittmaier, K. A. Friedrich, *Electrochim. Acta*, 2015, **151**, 332.
28 D. Wittmaier, S. Aisenbrey, N. Wagner, K. A. Friedrich, *Electrochim. Acta*, 2014, **149**, 355.
29 G. Du, X. Liu, Y. Zong, T. S. A. Hor, A. Yu, Z. Liu, *Nanoscale*, 2013, **5**, 4657.
30 L. J. Li, S. Y. Liu, A. Manthiram, *Nano Energy*, 2015, **12**, 852.
31 X. Wang, J. S. Lee, Q. Zhu, J. Liu, Y. Wang, S. Dai, *Chem. Mater.*, 2010, **22**, 2178.
32 B. Li, X. Ge, F. W. T. Goh, T. S. A. Hor, D. Geng, G. Du, Z. Liu, J. Zhang, X. Liu, Y. Zong, *Nanoscale*, 2015, **7**, 1830.
33 T. Yoon, Y. Park, *Nanoscale Res. Lett.*, 2012, **7**, 28.
34 J. Xiao, C. Chen, J. Xi, Y. Xu, F. Xiao, S. Wang, S. Yang, *Nanoscale*, 2015, **7**, 7056.
35 S. M. Abbas, S. T. Hussain, S. Ali, N. Ahmad, N. Ali, K. S. Munawar, *Electrochim. Acta*, 2013, **105**, 481.
36 H. Wang, T. Maiyalagan, X. Wang, *ACS Catal.*, 2012, **2**, 781.
37 F. W. T. Goh, Z. Liu, X. Ge, Y. Zong, G. Du, T. S. A. Hor, *Electrochim. Acta*, 2013, **114**, 598.
38 D. Yuan, J. Zeng, J. Chen, S. Tan, Y. Liu, N. Kristian, X. Wang, *J. Electrochem. Soc.*, 2009, **156**, B377.
39 M. Behrens, R. Schlögl, X-Ray Diffraction and Small Angle X-Ray Scattering: Characterization of Solid Materials and Heterogeneous Catalysts, Wiley-VCH Verlag GmbH & Co. KGaA, 2012, pp. 609.
40 K. Zhou, J. Liu, P. Wen, Y. Hu, Z. Gui, *Mater. Res. Bull*, 2015, **67**, 87.
41 J. Yang, H. Liu, W. N. Martens, R. L. Frost, *J. Phys. Chem. C*, 2010, **114**, 111.
42 A. J. Bard, L.R. Faulkner, Electrochemical Methods: Fundamentals and Applications, Wiley, New York, 2000.
43 C. Song, J. Zhang, Electrocatalytic Oxygen Reduction Reaction, in: J. Zhang (Ed.) PEM Fuel Cell Electrocatalysts and Catalyst Layers, Springer London, 2008, pp. 89.
44 A. Parthasarathy, S. Srinivasan, A. J. Appleby, C. R. Martin, *J. Electrochem. Soc.*, 1992, **139**, 2530.
45 T. Sharifi, G. Hu, X. Jia, T. Wågberg, *ACS Nano*, 2012, **6**, 8904.

Graphical Abstract:

Balancing the load of in-situ grown Co_3O_4 nanoparticles with their underneath N-doped Vulcan carbon powders is essential to produce scalable high-performance bifunctional catalysts for rechargeable Zn-air batteries.